Reduced-order modeling of modular, position-dependent systems with translating interfaces

Mechatronics 102 (2024) 103224

Contents lists available at ScienceDirect

Mechatronics

journal homepage: www.elsevier.com/locate/mechatronics

Reduced-order modeling of modular, position-dependent systems with translating interfaces☆

Robert A. Egelmeers [a], Lars A.L. Janssen [a,*], Rob H.B. Fey [a], Jasper W. Gerritsen [b], Nathan van de Wouw [a]

[a] Dynamics & Control, Department of Mechanical Engineering, Eindhoven University of Technology, The Netherlands
[b] ASMPT Center of Competency, Beuningen, The Netherlands

ARTICLE INFO

Keywords:
Complex dynamical systems
Position-dependent dynamics
Interconnected systems
Modular model framework
Modular model order reduction
Robust performance analysis

ABSTRACT

Many complex mechatronic systems consist of multiple interconnected dynamical subsystems, which are designed, developed, analyzed, and manufactured by multiple independent teams. To support such a design approach, a modular model framework is needed to reduce computational complexity and, at the same time, enable multiple teams to develop and analyze the subsystems in parallel. In such a modular framework, the subsystem models are typically interconnected by means of a static interconnection structure. However, many complex dynamical systems exhibit position-dependent behavior (e.g., induced by translating interfaces) which cannot be captured by such static interconnection models. In this paper, a modular model framework is proposed, which allows to construct an interconnected system model, which captures the position-dependent behavior of systems with translating interfaces, such as linear guide rails, through a position-dependent interconnection structure. Additionally, this framework allows to apply model reduction on subsystem level, enabling a more effective reduction approach, tailored to the specific requirements of each subsystem. Furthermore, we show the effectiveness of this framework on an industrial wire bonder. Here, we show that including a position-dependent model of the interconnection structure (1) enables to accurately model the dynamics of a system over the operating range of the system and, (2) modular model reduction methods can be used to obtain a computationally efficient interconnected system model with guaranteed accuracy specifications.

1. Introduction

Mechatronic systems often consist of multiple interconnected dynamical subsystems, which are designed individually and in parallel. An important subclass of such complex engineering systems can be modeled as multi-body systems consisting of flexible subsystems translating with respect to each other, in short, referred to as systems with translating interfaces. Examples of these systems are industrial wire bonder machines, printers and high-precision motion stages. Accurate, low-order models for the prediction of the motion and structural vibrations of such systems are essential to support model-based (controller) design and to support model-based diagnostics algorithms. Obtaining these models is challenged by (1) the large-scale nature of the models, (2) the interconnected nature of these systems, and (3) the position-dependent non-linearity induced by the translating interfaces, which is illustrated with an example in Fig. 1. The objective of this paper is to provide a modular modeling approach that also supports employing modular complexity reduction techniques such that low-order models with guaranteed accuracy specifications can be constructed that are accurate on the systems' entire operating range.

A common engineering approach is to construct a single high-order finite element (FE) model [1], containing all subsystems, to analyze the dynamical behavior of the system as a whole. However, to accommodate for increasing performance and accuracy demands, mechatronic systems are becoming increasingly complex. To enable the design of such complex system models, often, a modular approach is used, where the high-order system model is subdivided into multiple subsystem models that are interconnected through an interconnection structure. This enables the development and analysis of the subsystems in parallel by specialized design teams, before integrating them in the interconnected system design. In addition, such modular models also

☆ This paper was recommended for publication by Associate Editor Alessandro Beghi.

* Corresponding author.
E-mail addresses: robertegelmeers@outlook.com (R.A. Egelmeers), l.a.l.janssen@tue.nl (L.A.L. Janssen), r.h.b.fey@tue.nl (R.H.B. Fey), jasper.gerritsen@asmpt.com (J.W. Gerritsen), n.v.d.wouw@tue.nl (N. van de Wouw).

https://doi.org/10.1016/j.mechatronics.2024.103224
Received 19 February 2024; Received in revised form 23 May 2024; Accepted 10 June 2024
Available online 24 June 2024

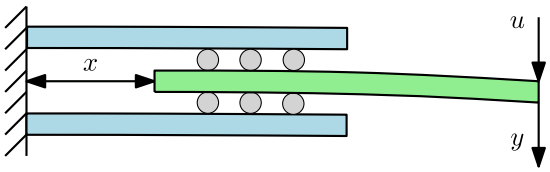

Fig. 1. Example of an interconnected system where the dynamic behavior from input u to output y is position-dependent, i.e., depends on x.

allow the reduction of the (computational) complexity of the interconnected system model. Such a modular modeling approach is commonly used in the systems and control field, e.g., [2,3]. Furthermore, in the structural dynamics field, dynamic substructuring techniques [4,5] and frequency-based substructuring methods [6] are also well-known modular modeling approaches.

Nowadays, such structural dynamics models of complex systems may contain millions of degrees of freedom (DOF), which makes their usage computationally infeasible. Therefore, the application of model order reduction (MOR) techniques is necessary to reduce the computational costs of evaluating the dynamical characteristics of these systems, related to specific input–output combinations and often in a certain frequency range of interest. Commonly used MOR techniques include, for instance, balancing methods [7], moment matching techniques [8–10], and Component Mode Synthesis (CMS) methods [11–13].

There exist two main approaches to reduce the complexity of *interconnected* system models: (1) MOR on the level of the interconnected system as a whole and (2) the reduced-order model (ROM) of each subsystem model is obtained individually without modifying the interconnection structure, after which the subsystem ROMs are interconnected. In contrast to the interconnected system level approach, a modular approach allows to apply different reduction techniques to each individual subsystem, tailored to the specific requirements of each subsystem [14]. Furthermore, the modular approach allows to make changes to individual subsystems without having to reconstruct the complete reduced-order model of the interconnected system. In this case, only the ROMs of the involved subsystems need to be reconstructed. Reduction on the level of interconnected system as a whole also typically does not preserve the interconnection structure. To address this challenge, structure-preserving methods have been developed [2,15–17]. Furthermore, a modular MOR approach provides a significant computational advantage, as it is more efficient to apply MOR to multiple smaller models compared to applying MOR on a single high-order interconnected model.

However, for modular MOR, predicting how the errors, introduced by the reduction of the subsystems, propagate through the ROM of the interconnected system as a whole is not trivial. Therefore, if subsystem models are reduced without considering the effect of subsystem modeling errors on the interconnected ROM, these errors may cause given frequency-response function (FRF) accuracy requirements of the interconnected ROM to be violated [18]. In [19], a mathematical framework is presented that enables to relate given, (external input to external output) FRF accuracy requirements of the ROM of the interconnected system to the FRF accuracy requirements of the subsystem ROMs. A necessary prerequisite for such approaches is the availability of a high-fidelity, modular and linear model accurately describing the (structural) dynamics of the system.

In many (mechatronic) applications, however, the input-to-output behavior is typically position-dependent, i.e., nonlinear, because their functionality requires that modules of the system translate with respect to each other. Examples of such systems include high-precision motion stages (e.g., gantry (wafer) stages, wire bonders), machine tools (e.g., CNC machines, drilling equipment), medical equipment (e.g., MRI-scanners, X-ray machines) or Cartesian robots. Models incorporating the position-dependent behavior of the system are crucial for

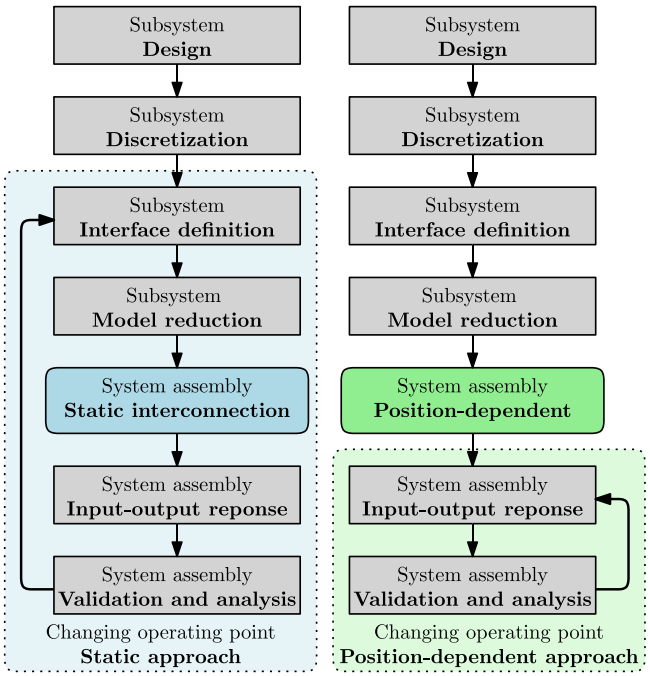

Fig. 2. Comparison of modeling workflows for position-dependent system models with, on the left, the standard static interconnection structure. On the right, the proposed position-dependent interconnection structure is given, which significantly reduces required effort for changing the operating points.

the purpose of designing the mechatronic system such that it performs according to specifications over the entire operating range of the system [20,21]. A common approach is to construct linearized models at certain operating points. These models can, however, only represent the dynamics locally at a certain position. Namely, if the subsystem positions change with respect to each other, then the subsystem models and the interface models need to be connected at different locations. This has immediate consequences for the (modular) complexity reduction of the subsystem models, since these typically highly depend on the input- and output-variables with which they interconnect to other subsystem models and the interface models. These challenges typically make the modeling (and complexity reduction) tasks highly time-consuming for the engineer and computationally expensive.

As a solution, existing methods to model position-dependent behavior of specific complex dynamic systems more efficiently include a position-dependent dynamic substructuring method for machine tools, specifically [22,23]. However, there is a need for general methods to construct reduced-order models of position-dependent interconnected systems with *translating* interfaces, such that, firstly, the models can accurately describe the dynamics of systems in the entire operating range of the systems and, secondly, FRF accuracy requirements of the interconnected system ROMs are guaranteed.

The main contribution of this paper is the development of a general modular model framework for the structural dynamics of systems with translating interfaces (such as, e.g., linear guide rails), that enables to incorporate a position-dependent interconnection structure. This is accomplished by introducing fixed grids of virtual interconnection points on the interfaces between subsystems, to be able to connect physical inputs and outputs. Physical characteristics (such as, for example, stiffness), specific to each interconnection, are interpolated between two adjacent virtual interconnection points on each interface, depending on their relative position to the physical interconnection. This eliminates the need to remodel and reapply MOR on the subsystem models when evaluating different operating points, saving a significant amount of manual and computational effort. The improved modeling workflow in

this framework, for systems that exhibit position-dependent behavior, is illustrated in Fig. 2.

Moreover, as an additional contribution of this paper, this position-dependent modeling approach is used in combination with the top-down modular MOR framework, described in [19], which also relies on a modular model framework where the subsystem models are interconnected through an interconnection structure. The method developed in [19], based on [24], guarantees the required FRF accuracy of the interconnected ROM based on the subsystem ROM FRFs accuracy. This leaves the position-dependent interconnection structure intact, such that the ROM of the interconnected system can be used to evaluate all operating points of interest. As a result, we provide a computationally efficient modular MOR framework for interconnected systems with position-dependent dynamics.

Finally, to evaluate the effectiveness of the proposed framework on real-world applications, a case study on an industrial wire bonder machine (WBM) is presented in this paper. A WBM, consisting of multiple modules/stages, makes wired interconnections between a semiconductor die and its packaging. In this case study, we show that including a position-dependent interconnection structure (1) enables to accurately model the dynamics of the WBM over the operating range of the system and, (2) modular model reduction methods guaranteeing assembly FRF accuracy specifications can still be used to obtain a computationally efficient model.

This paper is organized as follows. Section 2 gives the modular model framework of systems with a static interconnection structure. In Section 3, we show how this framework can be extended to enable a position-dependent interconnected system model. In Section 4, we concisely present the modular model reduction method. The effectiveness of the proposed position-dependent modeling and modular reduction framework is evaluated by means of a case study on an industrial wire bonder in Section 5. Finally, the conclusions are given in Section 6.

2. Modular model framework

In this section, we introduce the modular modeling framework that can be used for the purpose of decreasing computational costs, improving interpretability, and enabling an effective, structure-preserving model reduction approach. To obtain such a modular model, complex high-order (mechanical) systems can be subdivided into k, less complex, high-order subsystems $j \in \{1, \dots, k\}$, the dynamics of which can be described as second-order ordinary differential equations (ODE) of the form

$$M_j \ddot{q}_j(t) + D_j \dot{q}_j(t) + K_j q_j(t) = F_j(t), \tag{1}$$

where M_j, D_j, and K_j are the mass, damping and stiffness matrices of the respective subsystems with index j. The generalized coordinate and force vectors are denoted by $q_j(t)$ and $F_j(t)$, respectively. If we consider state $x_j(t) := \left[q_j^\mathsf{T}(t), \dot{q}_j^\mathsf{T}(t)\right]^\mathsf{T}$ and input $u_j(t) := F_j(t)$, we can formulate (1) into (descriptor) state-space form,

$$\begin{aligned} E_j \dot{x}_j(t) &= A_j x_j(t) + B_j u_j(t) \\ y_j &= C_j x_j(t) + D_{ss,j} u_j(t), \end{aligned} \tag{2}$$

of order n_j, i.e. $A \in \mathbb{R}^{n_j \times n_j}$, with n_j being the number of states of subsystem j, with inputs u_j and outputs y_j of dimensions m_j and p_j, respectively, and where

$$E_j = \begin{bmatrix} I & 0 \\ 0 & M_j \end{bmatrix}, \text{ and } A_j = \begin{bmatrix} 0 & I \\ -K_j & -D_j \end{bmatrix}. \tag{3}$$

In the input matrix B_j, the DOFs corresponding to the external inputs and interconnections with other subsystems are selected. In the output matrix C_j, the DOFs corresponding to the external outputs and interconnections with other subsystems are selected, and $D_{ss,j}$ is a direct feedthrough matrix. In the Laplace domain, the transfer functions $G_j(s)$, representing the input–output behavior of (2), are defined according to

$$G_j(s) = C_j \left(sE_j - A_j\right)^{-1} B_j + D_{ss,j}, \tag{4}$$

with $s \in \mathbb{C}$ as the Laplace variable. The subsystem transfer functions are collected in a block-diagonal transfer function

$$G_b(s) = \operatorname{diag}\left(G_1(s), \dots, G_k(s)\right), \tag{5}$$

with inputs $u_b = \left[u_1^\mathsf{T}, \dots, u_k^\mathsf{T}\right]^\mathsf{T}$ and outputs $y_b = \left[y_1^\mathsf{T}, \dots, y_k^\mathsf{T}\right]^\mathsf{T}$ of dimensions $m_b := \sum_{j=1}^k m_j$ and $p_b := \sum_{j=1}^k p_j$, respectively.

Next, the interaction between components is defined in order to derive the model of the interconnected system. One way to achieve this is by using a modular model framework [2,25], which is illustrated in Fig. 3. The subsystem models are interconnected according to

$$\begin{bmatrix} u_b \\ y_c \end{bmatrix} = \mathcal{K} \begin{bmatrix} y_b \\ u_c \end{bmatrix} := \begin{bmatrix} \mathcal{K}_{11} & \mathcal{K}_{12} \\ \mathcal{K}_{21} & \mathcal{K}_{22} \end{bmatrix} \begin{bmatrix} y_b \\ u_c \end{bmatrix}, \tag{6}$$

where u_b and y_b are used to connect the subsystems with each other, u_c and y_c are the external m_c inputs and p_c outputs of the interconnected system, and $\mathcal{K}$ is the (static) interconnection matrix.[1] The interactions between inputs and outputs of the subsystems are defined in $\mathcal{K}_{11}$. The inputs and outputs of the subsystems, that are chosen as external inputs and outputs, are selected in $\mathcal{K}_{12}$ and $\mathcal{K}_{21}$, respectively. Here, $\mathcal{K}_{22}$ can be seen as a direct feedthrough term from the external inputs to external outputs. Note that in many practical applications, the latter term is zero. The upper linear fractional transformation (LFT) of $G_b(s)$ and $\mathcal{K}$, defined as

$$G_c(s) = \mathcal{K}_{21} G_b(s) \left(I - \mathcal{K}_{11} G_b(s)\right)^{-1} \mathcal{K}_{12} + \mathcal{K}_{22}, \tag{7}$$

defines the transfer function $G_c(s)$ of order $n := \sum_{j=1}^k n_j$ from the external inputs u_c to the external outputs y_c of the interconnected system, see also Fig. 3.

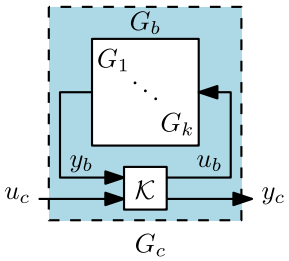

Fig. 3. Block diagram representation of the interconnected system $G_c(s)$ with subsystem models $G_1 \dots, G_k$, and the interconnection matrix $\mathcal{K}$.

3. Position-dependent modular model framework

In many dynamical systems, consisting of multiple interconnected subsystems, the subsystems are interconnected through translating interfaces, such as linear guide rails, to accommodate translation in a single direction. The interconnections between the subsystems with these translating interfaces are often represented by translational spring elements [26], which for instance may model the stiffness of rolling elements in the linear guide rails. In the standard framework, as visualized in the left part of Fig. 2, the (inputs and outputs of the) subsystem models G_j need to be reconstructed when the operating point is changed, after which the (momentary) interconnected system is constructed by interconnecting the subsystem models through a static interconnection matrix $\mathcal{K}$, as illustrated in Fig. 5(a). This process needs

[1] In case the external inputs and outputs are directly connected to a subsystem input and output, u_c and y_c contain identical elements in u_b and y_b, respectively.

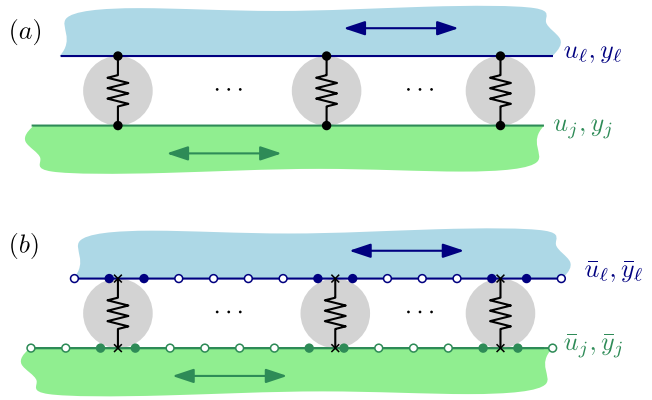

Fig. 4. Illustration of an interconnection structure between two arbitrary subsystems j and ℓ with a translating interface with (a) (physical) interconnection points for a specific operation point, and (b) position-dependent approach with a fixed grid of virtual interconnection points. Filled markers indicate virtual interconnections points that are active at a specific operating point, and used to interpolate the characteristics of each interconnection. Empty markers indicate currently inactive interconnection points.

to be repeated every time the operating point is changed (leading to a different $\mathcal{K}$ matrix) which makes such an approach computationally prohibitive in practice.

The physical interconnection points are continuously sliding along the interfaces and hence do not always coincide with the input–output pairs of the subsystem models, which are typically defined on discrete (and fixed) grid points at the interfaces. Therefore, for this class of position-dependent systems, we propose a novel method to construct the position-dependent model $\bar{G}_c$ (where the bar reflects that position-dependent nature of the model). To achieve this, we introduce:

1. Subsystem models $\bar{G}_j$ with fixed, virtual interface points.
2. A position-dependent interconnection matrix $\bar{\mathcal{K}}$.

Here, the key idea is to approximate the characteristics of each interconnection (the points at which the interconnection is active move as the bodies related to the translating interface move with respect to each other) by interpolation of the characteristics of connections, between fixed virtual interconnection points.

These virtual interconnection points are placed on a pre-defined grid along each substructure interface, as illustrated in Fig. 4(b). In this way, the subsystem models $\bar{G}_j$ are fixed for all operating points of the system while the interconnection matrix $\bar{\mathcal{K}}$ is position-dependent.

3.1. Constructing the position-dependent modular model

In the proposed position-dependent framework, the (inputs $\bar{u}_j$ and outputs $\bar{y}_j$ of the) subsystem models $\bar{G}_j$ for all $j \in \{1, \dots, k\}$ remain identical for changing operating points and are connected through a position-dependent interconnection matrix $\bar{\mathcal{K}}$, given by

$$\begin{bmatrix} \bar{u}_b \\ \bar{y}_c \end{bmatrix} = \bar{\mathcal{K}} \begin{bmatrix} \bar{y}_b \\ u_c \end{bmatrix} := \begin{bmatrix} \bar{\mathcal{K}}_{11} & \mathcal{K}_{12} \\ \mathcal{K}_{21} & \mathcal{K}_{22} \end{bmatrix} \begin{bmatrix} \bar{y}_b \\ u_c \end{bmatrix}. \tag{8}$$

Here, the subsystem inputs $\bar{u}_j$ and outputs $\bar{y}_j$ for all $j \in \{1, \dots, k\}$ are combined into $\bar{u}_b$ and $\bar{y}_b$ in the same way as u_b and y_b are constructed. Note that interconnection matrices $\mathcal{K}_{12}$, $\mathcal{K}_{21}$ and $\mathcal{K}_{22}$ are not affected by the position-dependent framework described in this section. Furthermore, a position-dependent transfer function from u_c to $\bar{y}_c$[2] of the interconnected system $\bar{G}_c$ can be constructed, defined by

$$\bar{G}_c(s) = \mathcal{K}_{21}\bar{G}_b(s)\left(I - \bar{\mathcal{K}}_{11}\bar{G}_b(s)\right)^{-1}\mathcal{K}_{12} + \mathcal{K}_{22}, \tag{9}$$

as illustrated in Fig. 5(b).

[2] The outputs $\bar{y}_c$ and y_c only differ in definition to be able to later compare the difference in the dynamics of the static and position-dependent models.

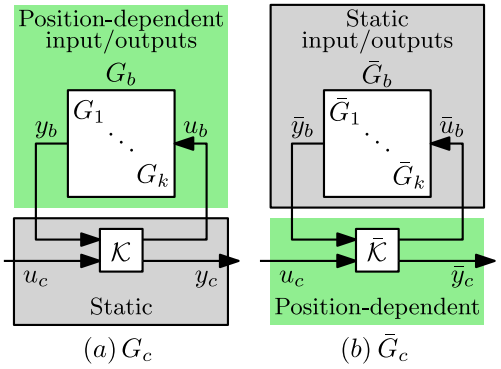

Fig. 5. Block-diagram representation of the interconnected system (a) G_c, i.e., with static interconnection matrix $\mathcal{K}$, and (b) $\bar{G}_c$, i.e., with position-dependent interconnection matrix $\bar{\mathcal{K}}$.

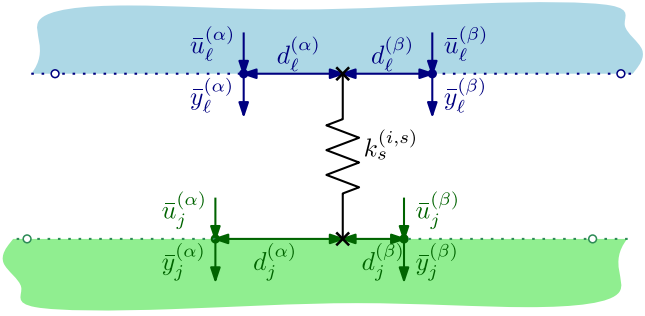

Fig. 6. Representation of a single physical interconnection point, interconnecting two arbitrary subsystems j and ℓ, with adjacent (i.e., active) virtual interconnection points on each side.

The position-dependent interconnection matrix $\bar{\mathcal{K}}_{11}$ is given by the sum of all interface interconnection matrices, defined by

$$\bar{\mathcal{K}}_{11} = \sum_{i=1}^{n_i} \bar{\mathcal{K}}_{11}^{(i)}. \tag{10}$$

Here, the interconnection between two subsystems at each interface $i \in \{1, \dots, n_i\}$, where n_i denotes the total number of interfaces in the system, can be modeled as an interface interconnection matrix $\bar{\mathcal{K}}_{11}^{(i)}$, which is defined by

$$\bar{\mathcal{K}}_{11}^{(i)} = \sum_{s=1}^{n_{i,s}} \bar{\mathcal{K}}_{11}^{(i,s)}, \tag{11}$$

i.e., as a summation of the spring interconnection matrix $\bar{\mathcal{K}}_{11}^{(i,s)}$ of each physical spring $s \in \{1, \dots, n_{i,s}\}$ at this interface, where $n_{i,s}$ is the number of springs at interface i. This single spring interconnection matrix $\bar{\mathcal{K}}_{11}^{(i,s)}$ is given by

$$\bar{\mathcal{K}}_{11}^{(i,s)} = P_u^{(i,s)} \hat{\mathcal{K}}_{11}^{(i,s)} P_y^{(i,s)\top} \in \mathbb{R}^{m_b \times p_b}, \tag{12}$$

where $P_u^{(i,s)} \in \mathbb{R}^{m_b \times 4}$ and $P_y^{(i,s)} \in \mathbb{R}^{4 \times p_b}$ are permutation matrices that define which virtual interconnection points are active. Entry (f, g) of $P_u^{(i,s)}$ is defined by

$$P_{u,(f,g)}^{(i,s)} = \begin{cases} 1, & \text{if } g = 1 \text{ and } \bar{u}_b^{(f)} \text{ corresponds to } \bar{u}_j^{(\alpha)} \\ 1, & \text{if } g = 2 \text{ and } \bar{u}_b^{(f)} \text{ corresponds to } \bar{u}_j^{(\beta)} \\ 1, & \text{if } g = 3 \text{ and } \bar{u}_b^{(f)} \text{ corresponds to } \bar{u}_\ell^{(\alpha)} \\ 1, & \text{if } g = 4 \text{ and } \bar{u}_b^{(f)} \text{ corresponds to } \bar{u}_\ell^{(\beta)} \\ 0, & \text{otherwise.} \end{cases} \tag{13}$$

Here, $\bar{u}_j^{(\alpha)}$, $\bar{u}_j^{(\beta)}$, $\bar{u}_\ell^{(\alpha)}$ and $\bar{u}_\ell^{(\beta)}$, are the nearest virtual interface points to the physical spring s on the interconnected subsystems $j \in \{1, \dots, k\}$

and $\ell \in \{1, \dots, k\}$, as illustrated in Fig. 6, and permutation matrix $P_y^{(i,s)}$ is defined equivalently to define the active outputs $\bar{y}_b$.

Furthermore, the elementary single spring interconnection matrix $\hat{\mathcal{K}}_{11}^{(i,s)}$ is given by

$$\hat{\mathcal{K}}_{11}^{(i,s)} = Q^{(i,s)} \begin{bmatrix} -k_s^{(i,s)} & k_s^{(i,s)} \\ k_s^{(i,s)} & -k_s^{(i,s)} \end{bmatrix} Q^{(i,s)\top} \in \mathbb{R}^{4\times 4}, \tag{14}$$

where $k_s^{(i,s)}$ is the translational stiffness of the specific physical spring and

$$Q^{(i,s)} = \begin{bmatrix} \frac{d_j^{(\alpha)}}{d_j^{(\alpha)}+d_j^{(\beta)}} & 0 \\ \frac{d_j^{(\beta)}}{d_j^{(\alpha)}+d_j^{(\beta)}} & 0 \\ 0 & \frac{d_\ell^{(\alpha)}}{d_\ell^{(\alpha)}+d_\ell^{(\beta)}} \\ 0 & \frac{d_\ell^{(\beta)}}{d_\ell^{(\alpha)}+d_\ell^{(\beta)}} \end{bmatrix} \in \mathbb{R}^{4\times 2}. \tag{15}$$

The linear interpolation matrix $Q^{(i,s)}$ determines how the interconnection between the interface points is distributed, based on the distances to the physical spring locations, given by $d_j^{(\alpha)}$, $d_j^{(\beta)}$, $d_\ell^{(\alpha)}$, and $d_\ell^{(\beta)}$, as illustrated in Fig. 6. With P and Q, the position-dependent behavior of the system is described. Note that this approach, for a single system position, is similar to typical approaches used when dealing with Finite Element non-conforming meshes [27].

Remark 1. In practice, for different positions of the subsystems, $\bar{\mathcal{K}}_{11}$ is a function of $P^{(i,s)}$ and $Q^{(i,s)}$, as $P^{(i,s)}$ determines which virtual interconnection points are active and $Q^{(i,s)}$ determines the extent in which these points are active. These matrices can be obtained automatically, as both $P^{(i,s)}$ and $Q^{(i,s)}$ are determined only by the relative position between the physical and virtual interconnection points. However, as an arbitrary number of virtual interconnection points can be selected and their positions can also be arbitrarily selected, it is not possible to provide a general position-dependent matrix formulation for $\bar{\mathcal{K}}_{11}$ given any position.

Summarizing, with this framework, the position-dependent interconnection matrix $\bar{\mathcal{K}}_{11}$ can approximate the behavior of an arbitrary number of physical springs $n_{i,s}$ on an interface i that are between virtual interface points. With $\bar{\mathcal{K}}_{11}$, the position-dependent interconnected system model $\bar{G}_c$ as in (9) can be obtained.

3.2. Accuracy of the position-dependent model

As the position-dependent model $\bar{G}_c$ uses interpolation (see (14), (15)) between a grid of virtual interconnection points to obtain a model of the physical interconnection between subsystems, a modeling error can be introduced. The size of this modeling error is dependent on several factors, including:

- **The number of virtual interconnection points**: If the number of virtual interconnection points increases, the distance between physical and virtual interconnection points decreases, which will typically lead to a decrease in modeling error. However, as already mentioned, increase of the number of virtual interconnection points also leads to an increase in complexity of the model, as the number of (virtual) inputs and outputs of the subsystems increases. This introduces a trade-off between accuracy and complexity of the model. In Section 5, we will address this trade-off on an industrial use case. It will be demonstrated that already with a relatively low number of virtual interconnection points, the error decreases quickly.
- **The stiffness of the subsystems**: The ratio between stiffness of the subsystems and the interface stiffness influences the accuracy of the position-dependent modeling approach. If this ratio is low, the interpolation using the virtual points can limit the accuracy of the model. If this ratio is high (as in the limit case for rigid bodies), the error introduced by the position-dependent modeling goes to zero. This is demonstrated by a simulation example, given in Appendix. We show that as the stiffness of the subsystems is increased, the difference in the input-to-output behavior between the models, converges to zero, regardless of the number of virtual interconnection points per interface in the position-dependent model.

Another factor influencing the accuracy is the total stroke length between the subsystems, as an increased stroke length generally leads to a higher position-dependency; this would typically also lead to a higher required number of virtual interconnections points. Finally, high-frequency eigenmodes are more prone to modeling errors using the virtual interconnection points. Therefore, it is important to clearly define the frequency range of interest for the model. In Section 5, these factors will be taken into account to determine the number and location of the virtual interconnection points on an industrial use case.

Remark 2. Note that in principle it is possible to extend the position-dependent framework by implementing higher-order interpolation in the interpolation matrix $Q^{(i,s)}$ in (15) with the potential of reducing the required number of virtual interconnection points. However, this would, as a trade-off, increase the complexity of the position-dependent interconnection matrix $\bar{\mathcal{K}}_{11}$. Note that this consideration is in many ways related to the decision of using linear or higher-order elements in finite-element methods (FEM), which has been widely studied [28].

4. Modular model order reduction

In this section, we show how to apply model order reduction to reduce the computational costs that are associated with the evaluation of the dynamical characteristics of the (position-dependent) interconnected system, either $G_c(s)$ or $\bar{G}_c(s)$.

As explained in the introduction, we apply *modular* MOR, i.e., reduction on subsystem level. By doing this, the high-order subsystem models, either $G_j(s)$, or $\bar{G}_j(s)$, of order n_j are reduced to the reduced-order subsystem models $\hat{G}_j(s)$ and $\hat{\bar{G}}_j(s)$, respectively, of order r_j, where, typically $r_j \ll n_j$. This reduction can be done using any MOR method that can achieve accurate subsystem ROMs $\hat{G}_j(s)$.

Next, the reduced-order interconnected system models $\hat{G}_c(s)$ or $\hat{\bar{G}}_c(s)$ of order $r := \sum_{j=1}^{k} r_j$ is constructed by interconnecting the subsystem ROMs $\hat{G}_j(s)$ or $\hat{\bar{G}}_j(s)$, respectively, through the same interconnection matrix as used in the construction of the high-order interconnected system. For the static $\mathcal{K}$ or the position-dependent $\bar{\mathcal{K}}$ interconnection matrix, the interconnected system ROMs $\hat{G}_c(s)$ and $\hat{\bar{G}}_c(s)$ can then simply be obtained using

$$\hat{G}_c(s) = \mathcal{K}_{21}\hat{G}_b(s)\left(I - \mathcal{K}_{11}\hat{G}_b(s)\right)^{-1}\mathcal{K}_{12} + \mathcal{K}_{22}, \text{ or} \tag{16}$$

$$\hat{\bar{G}}_c(s) = \mathcal{K}_{21}\hat{\bar{G}}_b(s)\left(I - \bar{\mathcal{K}}_{11}\hat{\bar{G}}_b(s)\right)^{-1}\mathcal{K}_{12} + \mathcal{K}_{22}, \tag{17}$$

respectively. In Fig. 7, a block-diagram representation of this approach for the proposed position-dependent modeling structure is illustrated.

To achieve sufficiently accurate models of the reduced interconnected system $\hat{G}_c(s)$, the accuracy of the subsystem ROMs $\hat{G}_j(s)$ needs to be sufficient. To achieve this, the modular MOR framework introduced in [19] is applied, which, in general terms, comprises the following aspects:

1. The required FRF accuracy of the ROM of the *interconnected system* $\hat{G}_c(s)$ with respect to the high-order interconnected system FRFs, i.e., from external inputs to external outputs, is determined by the system engineers.
2. Automatically, from these interconnected system FRF accuracy requirements, FRF accuracy requirements on the ROMs of the *subsystem* $\hat{G}_j$ are derived using μ-analysis, a methodology from the field of robust control.

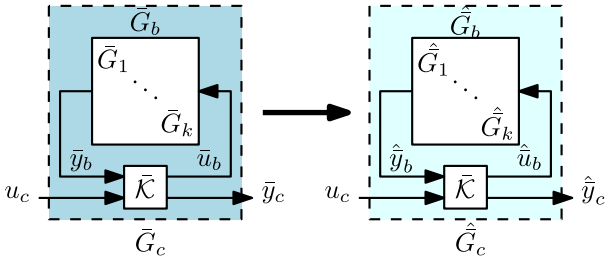

Fig. 7. Block diagram representation of the modular model order reduction approach the reduce the position-dependent interconnected model $\bar{G}_c(s)$ to a reduced-order interconnected model $\hat{\bar{G}}_c(s)$ by reducing the order of the independent subsystem models $\bar{G}_j(s)$, without altering the position-dependent interconnection matrix $\bar{\mathcal{K}}$.

3. When each of the computed subsystem ROMs satisfies its respective FRF accuracy requirements, the required accuracy on the interconnected system FRFs is guaranteed, hence allowing for a completely modular reduction of the subsystems.

This method can also be applied to the position-dependent models proposed in this paper to obtain accurate system ROMs $\hat{\bar{G}}_c(s)$. However, in this case, subsystem ROM accuracy requirements need to be validated in multiple positions of the system, as will be demonstrated in Section 5.

The method proposed in [19] relies heavily on the computation of FRFs of the high-order interconnected system. Computing this can be computationally expensive, especially when this needs to be done for many locations in the operating range of the position-dependent system. However, with the position-dependent modeling approach proposed in this paper, FRFs of the system can be cost-efficiently computed in the entire operating range of the system. Namely, computation of the FRF matrices is required for all subsystems $\bar{G}_j(s)$ only once because the FRFs of the subsystem models remain identical for every operating point. For every operating point, the position-dependent interconnection matrix $\bar{\mathcal{K}}_{11}$ simply needs to be obtained as described in Section 3. Then, the FRF matrices of the interconnected system can be determined according to (9) using computationally cheap matrix computations. In comparison, the conventional, static approach would require interface definition, model reduction, system assembly, and computation of the FRF of the assembly ROM at every operating point, as is illustrated in Fig. 2.

In the next section, we demonstrate that the position-dependent modeling framework can be used to efficiently generate accurate linear reduced-order models of an industrial wire bonder system over the entire operating range.

5. Use case of an industrial wire bonder machine

To illustrate the effectiveness of the proposed framework to approximate the position-dependent dynamics of an interconnected system using a single modular model, the proposed position-dependent framework is applied to a 3D-model of a wire bonder machine, which is illustrated in Fig. 8. For the purpose of achieving a high throughput and positioning-accuracy in the sub-micrometer range at the point of interest, it is crucial to predict the input-to-output behavior of the WBM's x-, y- and z-motion both fast and accurately. An accurate, low-complexity model for the WBM is essential to support model-based design and to support the design and online operation of control and diagnostic algorithms. Practice has shown, that the dynamic input-to-output behavior of the WBM depends on the relative positions of the flexible subsystems. Therefore, it is essential to construct a (modular) model of the WBM that accurately describes the changing dynamic behavior at different operating points of the stages.

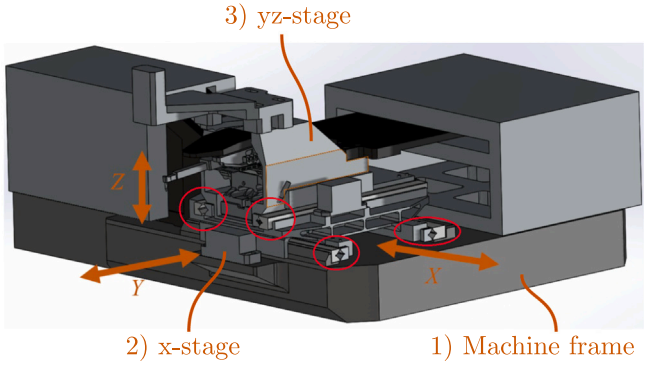

Fig. 8. (Simplified) 3D CAD model of the AB383 wire bonder from ASMPT. The locations of the cross-roller bearing rails are encircled in red.

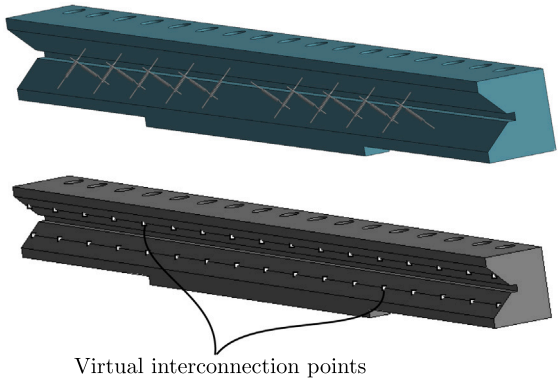

Fig. 9. Top: CAD model of one-half of a cross-roller bearing rail, wherein 18 translational springs (indicated by the 18 purple lines) represent the roller bearings. Bottom: CAD model of one-half of a cross-roller bearing rail, wherein a grid of ($n_v = 17$) equidistant virtual interconnection points is defined on each interface.

5.1. Modeling of the wire bonder machine

In this model, the wire bonder machine consists of three subsystems/modules: (1) the machine-frame, which is rigidly attached to the fixed-world at eight mounting points, (2) the x-stage, that is supported by the machine-frame using two cross-roller bearing rails (modeled by a cross-pattern of translational springs), which enables motion in the x-direction, and (3) the yz-stage, that is supported by the x-stage using two similar cross-roller bearing rails, which enables motion in the y-direction. The modules are indicated in Fig. 8. Furthermore, we consider three external (force) inputs and (displacement) outputs for this system. The three force inputs, which define u_c, are located at the positions of the motors, actuating, respectively, the x-, y- and z-direction. Actuation in the z-direction is realized by using an elastic rotational hinge around the x-axis. This hinge couples the y- and z-stage (together forming the yz-stage). It should be noted that in our case, we assume that rotations of the z-stage remain small enough to justify the assumption of linear behavior. The three displacement outputs, which define y_c, are measured at the encoder locations, enabling to monitor the motions of the x-, y- and z-stage.

In total, there are four cross-roller bearing rails present within the system, each containing nine roller bearings. Per rail, there are two pairs of interfaces lying opposite of each other in perpendicular directions. To each interface, nine translational springs, representing the roller bearings, are attached, as illustrated in the top CAD model in Fig. 9. Using Ansys [29], a grid of equally spaced virtual interconnection points is modeled on each interface, as is illustrated in the bottom CAD model in Fig. 9, where the total number of virtual interconnection points n_v is the same for each interface and varies between 9, 17,

Table 1
The number of DOFs per subsystem before reduction $n_{j,dof}$ and after reduction $r_{j,dof}$, and the cut-off frequencies $f_{c,j}$ that are associated with the CMS reduction of subsystems $j = 1, 2, 3$.

Σ_j	1	2	3
$f_{c,j}$ [-]	0.24	0.27	0.13
$n_{j,dof}$	$4.6 \cdot 10^5$	$1.6 \cdot 10^6$	$3.8 \cdot 10^6$
$r_{j,dof}$	347	431	329

and 33 for testing purposes. The DOFs that correspond to the virtual interconnection points, as well as the DOFs that correspond to the external inputs and outputs of the system are defined as interface DOFs.

Since the high-order FE-models of the subsystems Σ_j (of order n_j) consist of millions of DOFs, the subsystem models have to be reduced before exporting their respective (reduced) mass and stiffness matrices, such that they can be handled with a feasible amount of computational cost. To achieve this, the CMS reduction method of Craig-Bampton [11] is used, where the DOFs of the system are partitioned into boundary and internal DOFs. Two sets of modes are used. First, constraint modes (static modes) are defined for all interface DOFs, which were already defined earlier. Second, a set of kept fixed-boundary eigenmodes is defined, which are the kept dynamic modes of the system when all boundary DOFs are fixed. Both types of modes form the reduction-basis for this method.

After reduction, the boundary/interface DOFs are retained, while the internal DOFs are condensed to a (much) smaller set of generalized DOFs. The number of kept fixed-boundary eigenmodes, together with the number of boundary/interface DOFs, determines the order r_j of the reduced-order subsystem models.

For all subsystem models, 200 fixed-boundary eigenmodes are included in the reduction basis, such that the associated cut-off frequencies $f_{c,j}$, for all subsystems $j = 1, 2, 3$ are multiple times larger than the (normalized[3]) largest frequency of interest ($f_i = 0.04$ [–]) to ensure that this initial reduction step does not lead to a loss of accuracy in this frequency range.

The specific normalized cut-off frequencies, the number of DOFs before reduction $n_{j,dof}$, and the number of DOFs after reduction $r_{j,dof}$ (for $n_v = 9$), for all subsystems are given in Table 1. It is important to note that this initial CMS reduction step in general leads to reduced models which are still too big for some (especially real-time) applications. A second reduction step based on the modular reduction methodology in [19] will be discussed later in Section 5.3. By using the (reduced) mass and stiffness matrices M_j and K_j, respectively, damping matrices D_j for all subsystems $j = 1, 2, 3$ are constructed with 3% modal damping. Subsequently, state-space models are constructed for each subsystem using MATLAB [30], in which we exploit the sparse nature of the models. Note that all DOFs, associated with the virtual interconnection points, are defined as inputs and outputs in the input and output matrices B_j and C_j, respectively, in each subsystem model. Using the position-dependent modular model framework, as proposed in Section 3, a position-dependent interconnection matrix $\bar{\mathcal{K}} \in \mathbb{R}^{m_b \times p_b}$ is constructed to interconnect the subsystem models. In addition, the external inputs and outputs of the interconnected system are selected.

Furthermore, for validation purposes, the wire bonder system is also modeled at nine different operating points, using the static interconnection matrix $\mathcal{K}$ from Section 2, where the x- and y-positions of the x- and yz-motion stages are both varied between −0.02, 0, and 0.02 m. Note that constructing these separate models using the framework from Section 2 is significantly more time consuming than constructing a single position-dependent model, using the proposed methodology. In the next section, the position-dependent interconnected system model is compared to these fixed-position models.

[3] For confidentiality, all frequencies and FRF magnitudes are normalized.

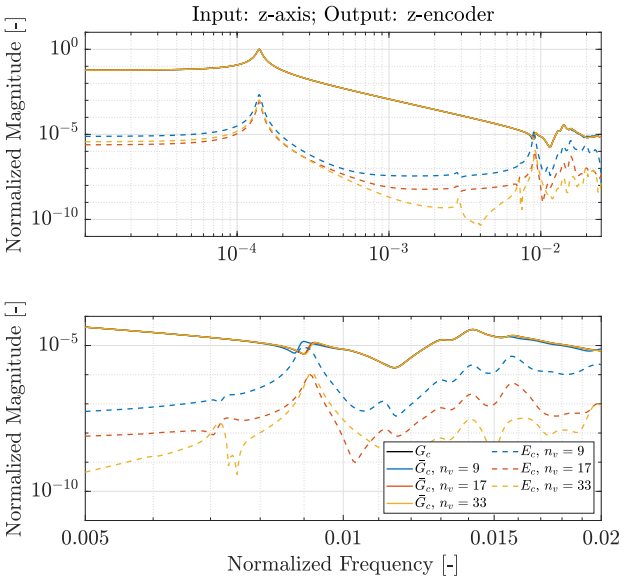

Fig. 10. Top figure: Comparison between the normalized magnitude plots $|G_{c,zz}(i\omega)|$ and $|\bar{G}_{c,zz}(i\omega)|$ for different amounts of virtual interconnection points per interface n_v, and the magnitude plots of the corresponding error dynamics $E_{c,zz}(i\omega)$ ($x = 0$ [m], $y = 0$ [m]). Bottom figure: Zoom of the higher normalized frequency range.

5.2. Comparing $\bar{G}_c$ with G_c

In Fig. 10, the normalized magnitude of $G_{c,zz}$ (external z-actuator input to external z-encoder output) of the interconnected system model, constructed with the static interconnection matrix $\mathcal{K}$, is compared to the interconnected system models, constructed with the position-dependent interconnection matrix $\bar{\mathcal{K}}$ for different numbers of virtual interconnection points n_v per interface. From Fig. 10, it can be observed that the modular modeling approach is able to accurately approximate the dynamics.

There is a significant difference in magnitude between the model $G_{c,zz}$ and the model $\bar{G}_{c,zz}$ for $n_v = 9$. In contrast, this difference is significantly less apparent for $n_v = 17$ and $n_v = 33$. By inspecting the error dynamics $E_{c,zz}(s) = G_{c,zz}(s) - \bar{G}_{c,zz}(s)$, it can be observed that if the number of virtual interconnection points per interface n_v is increased, the accuracy of position-dependent model $\bar{G}_{c,zz}(s)$ increases. This is expected, because for an increasing number virtual interconnection points per interface, the (interpolation) distances between the physical interconnection point and the adjacent virtual interconnection points become smaller, resulting in a more accurate approximation of the interface dynamics.

To demonstrate the computational advantages of using the proposed model framework over the static model framework, in Fig. 11, the normalized magnitudes of the FRFs of $\bar{G}_{c,zy}$ (external y-actuator input to external z-encoder output) are shown as a function of the operating point in the x- and y-direction, respectively. Here, a grid of 50 x- and y-positions are used, respectively. It is computationally (relatively) inexpensive to generate these results with the proposed framework, as the FRFs of the subsystems are required to be computed only once. Then, the FRFs of the interconnected system can be determined for a large number of operating points in fast succession, using cheap matrix operations, as discussed in Section 3. In comparison, the conventional approach would require computation of new FRFs from the subsystem models at every operating point. Fig. 11 also shows that such analysis can quickly visualize how resonance frequencies (e.g., the one near the normalized frequency of 0.01) depend on the y-position, while for the x-position it shows no significant position-dependent behavior.

To demonstrate the accuracy of the position-dependent modular model framework, entries of $G_c(s)$ are compared to similar entries from $\bar{G}_c(s)$ at multiple operating points using $n_v = 17$. In Figs. 12 and 13,

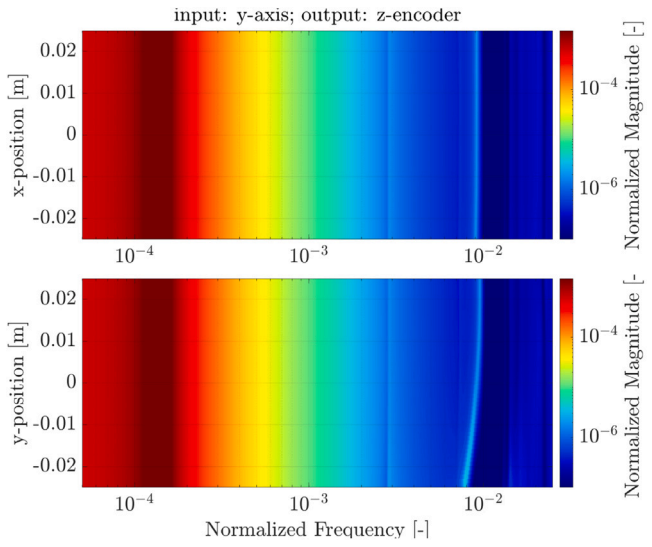

Fig. 11. Normalized magnitude plot $|\bar{G}_{c,zy}(i\omega)|$ as a function of a changing operating point in the x-direction ($y = 0$ [m], top figure) and as a function of a changing operating point in the y-direction ($x = 0$ [m], bottom figure).

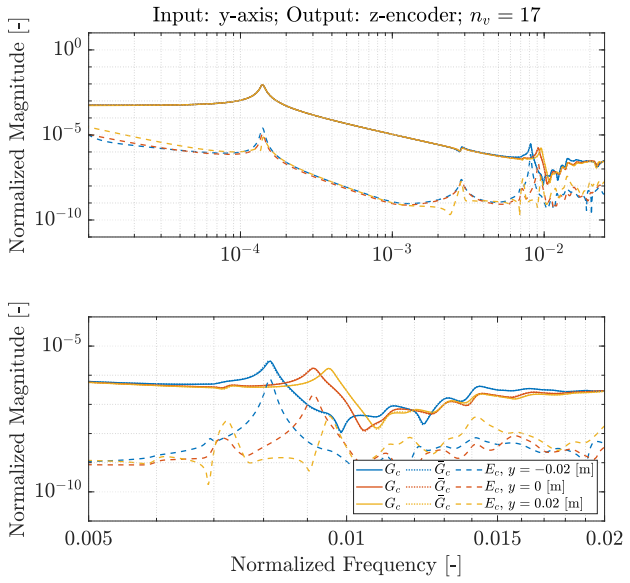

Fig. 12. Top figure: Comparison between the normalized magnitude plots $|G_{c,zy}(i\omega)|$ and $|\bar{G}_{c,zy}(i\omega)|$ for different operating points in the y-direction, including the magnitude plots of the corresponding error dynamics $E_{c,zy}(i\omega)$ ($x = 0$ [m]). Bottom figure: Zoom of the higher normalized frequency range.

the normalized magnitudes of the FRFs of both models are plotted along with the normalized magnitudes of the FRFs of the corresponding error dynamics $E_c(s) = G_c(s) - \bar{G}_c(s)$, for the transfer functions from the actuator input y to encoder output z, and from actuator input z to encoder output z, respectively. It can be observed that the wire bonder model shows a clear sensitivity to a changing operating point in the y-direction ($x = 0$ [m] in Figs. 12 and 13, with regards to its input-to-output behavior, at higher frequencies.

Moreover, it appears that for each operating point, the plotted entries of $G_c(s)$ can be closely approximated by $\bar{G}_c(s)$ with sufficient accuracy. In Figs. 14 and 15, the normalized magnitudes of the FRFs of $G_c(s)$, $\bar{G}_c(s)$, and $E_c(s)$, are plotted for the same inputs and outputs for multiple operating points in the x-direction ($y = 0$ [m]). It can be observed that the wire bonder is significantly less sensitive to a changing operating point in the x-direction, with regards to its input-to-output behavior. Also in Figs. 14 and 15, the position-dependent

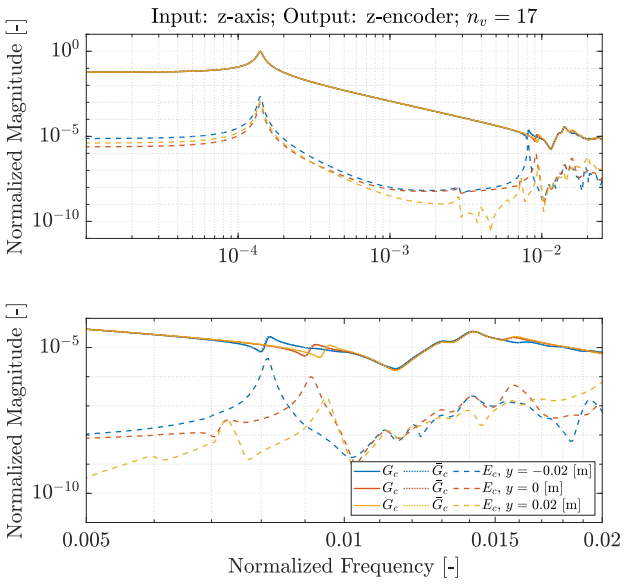

Fig. 13. Top figure: Comparison between the normalized magnitude plots $|G_{c,zz}(i\omega)|$ and $|\bar{G}_{c,zz}(i\omega)|$ for different operating points in the y-direction, including the magnitude plots of the corresponding error dynamics $E_{c,zz}(i\omega)$ ($x = 0$ [m]). Bottom figure: Zoom of the higher normalized frequency range.

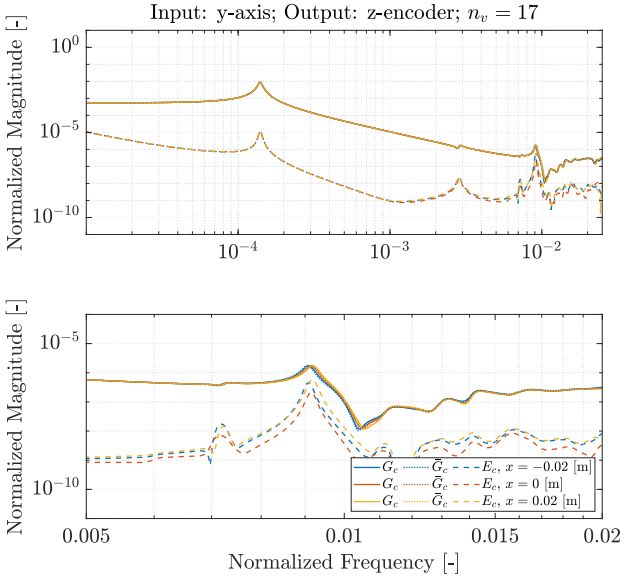

Fig. 14. Top figure: Comparison between the normalized magnitude plots $|G_{c,zy}(i\omega)|$ and $|\bar{G}_{c,zy}(i\omega)|$ for different operating points in the x-direction, including the magnitude plots of the corresponding error dynamics $E_{c,zy}(i\omega)$ ($y = 0$ [m]). Bottom figure: Zoom of the higher normalized frequency range.

interconnected system model $\bar{G}_c(s)$ is able to approximate $G_c(s)$ with sufficient accuracy.

5.3. Modular model reduction

Even though the resulting position-dependent interconnected system model $\bar{G}_c$, after the initial CMS reduction step, is of a sufficiently small order to analyze the input-to-output behavior of the WBM, it is still of a relatively high-order ($n = 2166$ for $n_v = 9$ virtual interconnection points per interface). Therefore, we aim to further reduce the interconnected system model, without compromising too much on model accuracy. A modular MOR framework that allows this is recently introduced in [19]. This framework enables to determine FRF accuracy requirements on the subsystem ROMs, such that we can guarantee

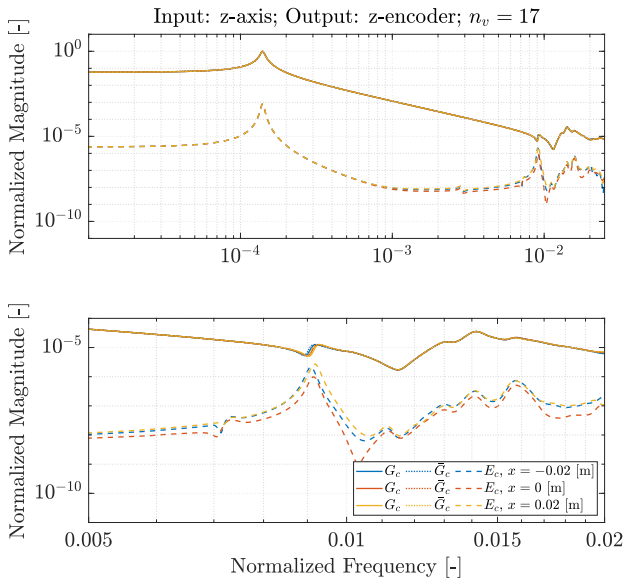

Fig. 15. Top figure: Comparison between the normalized magnitude plots $|G_{c,zz}(i\omega)|$ and $|\bar{G}_{c,zz}(i\omega)|$ for different operating points in the x-direction, including the magnitude plots of the corresponding error dynamics $E_{c,zz}(i\omega)$ ($y = 0$ [m]). Bottom figure: Zoom of the higher normalized frequency range.

FRF error bounds on the interconnected system ROM. Furthermore, this framework allows to use multiple MOR techniques, tailored to the specific requirements on each subsystem. This way, only a single ROM needs to be computed for each subsystem, which can be used to obtain accurate system models over the entire operating point of the WBM. In contrast, the conventional approach would require a dedicated reduction step for each operating point. This difference is also illustrated in Fig. 2. In this second reduction step, we use three different MOR techniques: (1) Balanced truncation [8], (2) Craig-Bampton CMS [11], and 3) Hintz–Herting CMS [12].

Since we made the interconnected system model position-dependent through $\bar{\mathcal{K}}$, it is a priori unclear how this position-dependency affects the minimal model order that is required, such that a specific FRF accuracy requirement of the ROM $\hat{\bar{G}}_c(s)$ is met at all operating points. Therefore, we apply the MOR framework from [19] to reduce $\bar{G}_c(s)$ at nine different operating points. For each operating point, the minimal subsystem model order r_j is determined for all three reduction techniques, such that the interconnected system model accuracy requirements are based on a maximum on the relative error of 10% up until the largest frequency of interest ($f_i = 0.04$ [-]), i.e.,

$$\frac{|\hat{\bar{G}}_{c,zy}(i\omega) - \bar{G}_{c,zy}(i\omega)|}{|\bar{G}_{c,zy}(i\omega)|} < 0.1. \tag{18}$$

for all ω in the frequency range of interest.

Since the MOR framework from [19] does not scale efficiently with large interconnection matrices (it does scale with a high number of system states), we use $n_v = 9$ to limit the required computation time, which gives $\bar{\mathcal{K}} \in \mathbb{R}^{308\times308}$. This results in a computation time of 116 minutes per evaluated operating point (AMD(R) Ryzen(TM) 7 5800X3D CPU (4.5 GHz), 64 GB RAM). The results are presented in Table 2.[4]

From the results, it can be concluded that there is little variation in the minimally required subsystem model orders between the operating points, when using the same reduction technique. This indicates that, in this case study, the accuracy requirements of the subsystems are not very sensitive to the operating point of the system. Furthermore, it can be concluded that the balanced truncation method is the most effective MOR technique for the first and second subsystem models, whereas the CMS method of Hintz–Herting is the most effective MOR technique for the third subsystem. In Table 3, the resulting subsystem model orders, before and after reduction, are presented.

These results show that the MOR framework, introduced in [19], in combination with the position-dependent model introduced in this paper allows to construct an accurate, modular, and position-dependent ROM of the interconnected system model that facilitates to obtain FRFs at the operating range of the interconnected system in a fast and accurate manner.

Table 2
Minimal subsystem model orders r_j (number of states) to meet the accuracy requirements of the interconnected system model, evaluated at nine different operating points, using three MOR techniques.

		Operating point								
		1	2	3	4	5	6	7	8	9
Σ_1	BT	118	118	118	118	118	118	118	118	118
	CB	162	162	166	166	166	166	178	178	170
	HH	162	162	162	162	162	174	170	166	166
Σ_2	BT	252	252	252	252	252	252	253	253	253
	CB	434	434	434	434	434	434	434	434	434
	HH	334	334	334	338	334	350	342	342	342
Σ_3	BT	328	328	328	328	328	328	328	328	328
	CB	332	332	332	332	332	332	332	332	332
	HH	240	240	240	240	240	240	252	248	248

Table 3
Optimal MOR technique and model order r_j per subsystem to meet the accuracy requirements of the interconnected system model at all nine operating points.

	Method	n_j	r_j	Reduction %
Σ_1	BT	646	118	80.8
Σ_2	BT	862	253	70.6
Σ_3	HH	658	252	61.7
Total:		2166	623	71.2

6. Conclusions

In conclusion, this paper introduces a novel modular model framework for position-dependent dynamical systems consisting of multiple flexible bodies and translating interfaces, while addressing a key limitation in current modeling approaches. Namely, the conventional modular model framework requires remodeling of subsystems when evaluating the input-to-output behavior at different operating points (due to the position-dependency), which often has to be done manually and/or is computationally costly. The proposed framework overcomes this roadblock by incorporating a position-dependent interconnection structure through fixed grids of virtual interconnection points, introduced along the interfaces. This ensures that the subsystem models are identical at all operating points of the system.

In addition, by making the interconnection structure position-dependent, the proposed framework enables the construction of a modular reduced-order model for the interconnected system that incorporates position-dependent behavior without sacrificing modularity. To obtain this reduced-order model, we use a recently introduced modular model-order reduction framework that ensures that FRF error bounds on the reduced-order model of the interconnected system are satisfied (at a selection of operating points), enhancing the reliability and applicability of the proposed modular model framework.

Finally, the proposed modular modeling framework is applied to an industrial wire bonder model, in which we demonstrate the modeling method. Here, we validate by comparison with the classical modeling

[4] It should be noted that we can only guarantee the aforementioned accuracy requirement on $\hat{\bar{G}}_c(s)$ for the nine operating points that were evaluated using the reduced subsystem models orders given in Table 2, which express (for different reduction methods) the minimal subsystem ROM order, such that automatically (18) is satisfied.

approach that the model is accurate when enough virtual interconnection points are used. We show, for this case study, an accurate, modular, and position-dependent reduced-order model that can be used to obtain frequency-response functions at the operating range of the system in a fast and accurate manner. Such models can subsequently be used to support model-based design guaranteeing performance over the entire operating range.

CRediT authorship contribution statement

Robert A. Egelmeers: Writing – original draft, Visualization, Validation, Software, Methodology, Investigation, Formal analysis, Data curation, Conceptualization. **Lars A.L. Janssen:** Writing – review & editing, Writing – original draft, Visualization, Validation, Supervision, Software, Project administration, Methodology, Investigation, Formal analysis, Data curation, Conceptualization. **Rob H.B. Fey:** Writing – review & editing, Validation, Supervision, Project administration, Methodology, Conceptualization. **Jasper W. Gerritsen:** Writing – review & editing, Validation, Supervision, Project administration, Methodology, Conceptualization. **Nathan van de Wouw:** Writing – review & editing, Validation, Supervision, Project administration, Methodology, Conceptualization.

Declaration of competing interest

The authors declare the following financial interests/personal relationships which may be considered as potential competing interests: Lars A. L. Janssen reports financial support was provided by Dutch Research Council. If there are other authors, they declare that they have no known competing financial interests or personal relationships that could have appeared to influence the work reported in this paper.

Data availability

The data that has been used is confidential.

Acknowledgments

This publication is part of the project Digital Twin with project number P18-03 of the research programme Perspectief which is (mainly) financed by the Dutch Research Council (NWO).

Appendix. Preservation of stiffness properties

In this section, we demonstrate that, for a certain operating point, the translational and rotational stiffness (with respect to an arbitrary point on the interface) of the position-dependent interconnection matrix $\bar{\mathcal{K}}_{11}$, is equivalent to the static interconnection matrix $\mathcal{K}_{11}$. Consider the interconnected system $G_c(s)$, interconnected through a static interconnection matrix $\mathcal{K}$, and $\bar{G}_c(s)$, interconnected through a position-dependent interconnection matrix $\bar{\mathcal{K}}$. In the simulation example below we show that when the stiffness of the subsystems is increased, the difference in input-to-output behavior between $G_c(s)$ and $\bar{G}_c(s)$ converges to zero. However, in practice the subsystems are flexible. Therefore, errors are introduced by interpolating the characteristics of the physical interconnections to the inputs and outputs, corresponding to the virtual interconnection points, as described in Section 3.

Using a simplified 2D FE-model of the WBM, we demonstrate that, for an increasing subsystem stiffness, the error between the FRFs of $G_c(s)$ and $\bar{G}_c(s)$ converges to zero. The WBM in this model (illustrated in Fig. A.16) consists of two subsystems: (1) the x-stage, which is modeled as a clamped beam, because there are no DOFs in the x-direction, and (2) the yz-stage, that is supported by the x-stage using three bearings (modeled by three vertical translational springs with stiffness $k_s = 2{\cdot}10^6$ [N/m]), which enables motion in the y-direction. Furthermore, the horizontal dimensions of the yz-stage are stretched in this model to exaggerate position-dependent behavior (see Fig. A.17).

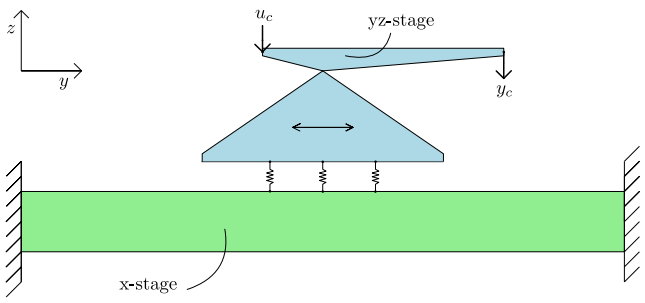

Fig. A.16. 2D wire bonder model, consisting of an x-stage and a yz-stage (with external input u_c and output y_c), which are interconnected by three bearings (modeled as translational springs).

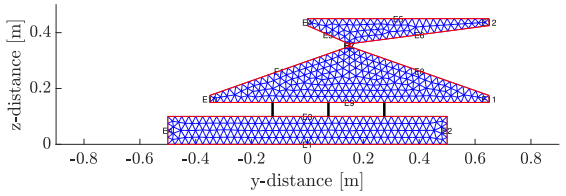

Fig. A.17. 2D FE models of the x-stage and yz-stage of the WBM, interconnected through three translational springs (indicated by black vertical lines between the subsystems).

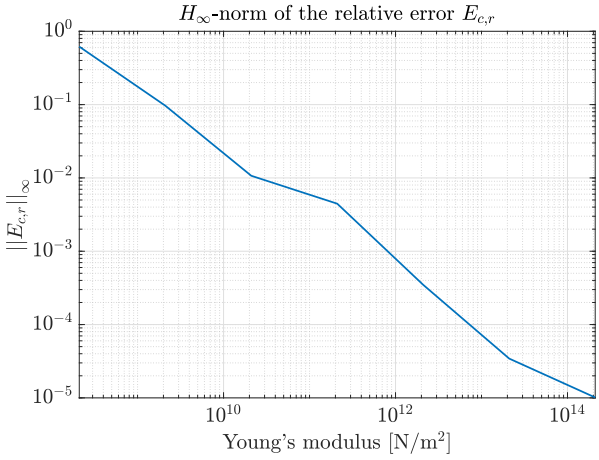

Fig. A.18. Plot of the H_∞ norm of the relative error FRF $E_{c,r}(i\omega)$, as a function of the Young's modulus of the subsystems.

Using MATLAB's [30] PDE toolbox, FE-models of the subsystems have been generated (see Fig. A.17), where both are discretized using quadratic triangular plane-stress elements, with a mass density of 7800 kg/m^2, a Poisson's ratio of 0.3, and 3% modal damping. The Young's modulus is treated as a variable in this example to vary the stiffness of the subsystems. The interconnected system models $G_c(s)$ and $\bar{G}_c(s)$ (with $n_v = 5$ virtual interconnection points per interface) have been constructed according to the modular model frameworks from Sections 2 and 3, respectively.

To quantify the accuracy of the FRF of $\bar{G}_c(s)$ compared to the FRF of $G_c(s)$, as a function of the subsystem stiffness, the H_∞ norm of the relative error $E_{c,r}(s)$ is calculated according to

$$\left\|E_{c,r}(s)\right\|_\infty = \left\|\frac{\bar{G}_c(s) - G_c(s)}{G_c(s)}\right\|_\infty = \max_{\omega\in\mathbb{R}} \left|E_{c,r}(i\omega)\right|. \tag{A.1}$$

The results are plotted in Fig. A.18. It can be observed that the norm of the relative error FRF $E_{c,r}(i\omega)$ converges to zero when the subsystem

stiffness is increased. This indicates that when the subsystems behave as rigid bodies, the static and position-dependent interconnection matrices $\mathcal{K}$ and $\bar{\mathcal{K}}$, respectively, have an identical effect on the input-to-output behavior of the interconnected system. This implies that the stiffness, described by the position-dependent interconnection structure, is preserved in the position-dependent model framework, described in Section 3. In real-world applications, the subsystems do not behave as rigid-bodies, and, therefore, the error between $G_c(s)$ and $\bar{G}_c(s)$ can only be decreased by adding more virtual interconnection points on each interface (or by placing them more efficiently).

References

[1] Hughes Thomas JR. The finite element method: linear static and dynamic finite element analysis. Courier Corporation; 2012.
[2] Sandberg Henrik, Murray Richard M. Model reduction of interconnected linear systems. Optim Control Appl Methods 2009;30(3):225–45.
[3] Vaz AF, Davison Edward J. Modular model reduction for interconnected systems. Automatica 1990;26(2):251–61.
[4] Craig Jr Roy R. Coupling of substructures for dynamic analyses-an overview. In: 41st Structures, structural dynamics, and materials conference and exhibit. 2000, p. 1573.
[5] Rixen DanielJ. A dual craig–bampton method for dynamic substructuring. J Comput Appl Math 2004;168(1–2):383–91.
[6] de Klerk Dennis, Rixen Daniel J, Voormeeren SN. General framework for dynamic substructuring: history, review and classification of techniques. AIAA J 2008;46(5):1169–81.
[7] Gugercin Serkan, Antoulas Athanasios C. A survey of model reduction by balanced truncation and some new results. Internat J Control 2004;77(8):748–66.
[8] Antoulas Athanasios C. Approximation of large-scale dynamical systems. Philadelphia: SIAM; 2005.
[9] Lanczos Cornelius. An iteration method for the solution of the eigenvalue problem of linear differential and integral operators. J Res Natl Bur Stand 1950;45(4).
[10] Arnoldi Walter Edwin. The principle of minimized iterations in the solution of the matrix eigenvalue problem. Quart Appl Math 1951;9(1):17–29.
[11] Craig Jr Roy R, Bampton Mervyn CC. Coupling of substructures for dynamic analyses. AIAA J 1968;6(7):1313–9.
[12] Herting DN. A general purpose, multi-stage, component modal synthesis method. Finite Elem Anal Des 1985;1(2):153–64.
[13] Rubin S. Improved component-mode representation for structural dynamic analysis. AIAA J 1975;13(8):995–1006.
[14] Reis Timo, Stykel Tatjana. A survey on model reduction of coupled systems. Model order reduction: Theory. Res Aspects Appl 2008;133–55.
[15] Vandendorpe Antoine, Van Dooren Paul. Model reduction of interconnected systems. In: Model order reduction: theory, research aspects and applications. Springer; 2008, p. 305–21.
[16] Lutowska Agnieszka. Model order reduction for coupled systems using low-rank approximations [Ph.D. thesis], Eindhoven University of Technology; 2012.
[17] Poort Luuk, Besselink Bart, Fey Rob HB, van de Wouw Nathan. 56, (2):2023, p. 4240–5,
[18] Yeung Enoch, Gonçalves Jorge, Sandberg Henrick, Warnick Sean. The meaning of structure in interconnected dynamic systems. 2011, arXiv preprint arXiv:1108.2755.
[19] Janssen Lars AL, Besselink Bart, Fey Rob HB, van de Wouw Nathan. Modular model reduction of interconnected systems: A top-down approach. IFAC-PapersOnLine 2023;56(2):4246–51.
[20] da Silva Maíra M, Desmet Wim, Van Brussel Hendrik. Design of mechatronic systems with configuration-dependent dynamics: simulation and optimization. IEEE/ASME Trans Mechatronics 2008;13(6):638–46.
[21] da Silva Maíra M, Brüls Olivier, Desmet Wim, Van Brussel Hendrik. Integrated structure and control design for mechatronic systems with configuration-dependent dynamics. Mechatronics 2009;19(6):1016–25.
[22] Law Mohit, Ihlenfeldt Steffen. A frequency-based substructuring approach to efficiently model position-dependent dynamics in machine tools. Proc Inst Mech Eng Part K 2015;229(3):304–17.
[23] Liu Yen-Po, Altintas Yusuf. Predicting the position-dependent dynamics of machine tools using progressive network. Precis Eng 2022;73:409–22.
[24] Janssen Lars AL, Besselink Bart, Fey Rob HB, van de Wouw Nathan. Modular model reduction of interconnected systems: A robust performance analysis perspective. Automatica 2024;160:111423.
[25] Janssen Lars AL, Besselink Bart, Fey Rob HB, Abbasi Mohammad Hossein, van de Wouw Nathan. A priori error bounds for model reduction of interconnected linear systems using robust performance analysis. In: 2022 American control conference. 2022, p. 1867–72.
[26] Chang Jyh-Cheng, Hung JP. Analytical and finite element modeling of the dynamic characteristics of a linear feeding stage with different arrangements of rolling guides. Math Probl Eng 2014;2014:1–11.
[27] Kumar Ashok V, Buria Ravi, Padmanabhan Sanjeev, Gu Linxia. Finite element analysis using nonconforming mesh. J Comput Inf Sci Eng 2008;8. 031005–1.
[28] Shewchuk Jonathan. What is a good linear finite element? - interpolation, conditioning, anisotropy, and quality measures. In: Proceedings of the 11th international meshing roundtable. vol. 73, 2002.
[29] Ansys Inc. Mechanical version: (2021 R1). 2023.
[30] MathWorks Inc. Matlab version: (r2023a). 2023.

Robert A. Egelmeers was born in Veghel, the Netherlands, in 1997. He received his M.Sc.-degree in Mechanical Engineering from the Eindhoven University of Technology, Eindhoven, the Netherlands in 2023. Currently, he is working as a Factory Engineer within the company VDL ETG Eindhoven B.V, seconded by the company Evoke B.V. His fields of interest include structural dynamics, model reduction, and control of mechatronic systems.

Lars A.L. Janssen was born in Nijmegen, the Netherlands, in 1996. He received his M.Sc.-degree (cum laude) in Mechanical Engineering from the Eindhoven University of Technology, Eindhoven, The Netherlands in 2019. He obtained his Ph.D.-degree (cum laude) at the Dynamics and Control (DC) group of the Mechanical Engineering Department at Eindhoven University of Technology (TU/e). His current research interest are large-scale interconnected systems, modeling of complex systems and structures, model reduction, and systems engineering.

Rob H.B. Fey received his M.Sc. degree (cum laude) in Mechanical Engineering and his Ph.D. degree from Eindhoven University of Technology in The Netherlands, in 1987 and 1992, respectively. He was a recipient of the Shell Study Prize for his Ph.D. thesis. From 1992 to 2002, he was a Senior Scientist with the Structural Dynamics Group of The Netherlands Organization for Applied Scientific Research (TNO) in Delft, The Netherlands Since 2002, he has been with the Dynamics & Control Group, Department of Mechanical Engineering, Eindhoven University of Technology, where he currently is an Associate Professor of Structural Dynamics. He is (co-)author of many refereed journal papers, chapters in books, and conference papers. His general research interests include the modeling, analysis, and validation of the dynamic behavior of complex structures and (multiphysics) systems. Current focus is on data- and AI-based model updating techniques and model reduction of interconnected systems. His main applications are currently in the fields of High-Tech Systems, Mechatronic Systems and Micro-ElectroMechanical Systems. He is member of the Editorial Board of the Journal of Vibration and Control and the Technical Committee for Vibrations of IFToMM. He was guest editor of the journal Nonlinear Dynamics.

Jasper W. Gerritsen obtained his M.Sc. degree in 2022 in Mechanical Engineering of the University of Twente (UT) located in Enschede, the Netherlands. His study was specialized in the field of flexible multibody dynamics at the department of Applied Mechanics and Data Analysis. Currently, he is working at the ASMPT Center of Competency in Beuningen, the Netherlands as a mechatronics engineer focusing on modeling and system identification of dynamical systems for back-end machines in the semiconductor industry.

Nathan van de Wouw obtained his M.Sc.-degree (with honours) and Ph.D.-degree in Mechanical Engineering from the Eindhoven University of Technology, The Netherlands, in 1994 and 1999, respectively. He currently holds a full professor position at the Mechanical Engineering Department of the Eindhoven University of Technology, The Netherlands. He has been working at Philips Applied Technologies, The Netherlands, in 2000 and at The Netherlands Organisation for Applied Scientific Research, The Netherlands, in 2001. He has been a visiting professor at the University of California Santa Barbara, U.S.A., in 2006/2007, at the University

of Melbourne, Australia, in 2009/2010 and at the University of Minnesota, U.S.A., in 2012 and 2013. He has held a (part-time) full professor position the Delft University of Technology, The Netherlands, from 2015–2019. He has also held an adjunct full professor position at the University of Minnesota, U.S.A, from 2014–2021. He has published the books 'Uniform Output Regulation of Nonlinear Systems: A convergent Dynamics Approach' with A.V. Pavlov and H. Nijmeijer (Birkhauser, 2005) and 'Stability and Convergence of Mechanical Systems with Unilateral Constraints' with R.I. Leine (Springer-Verlag, 2008). In 2015, he received the IEEE Control Systems Technology Award "For the development and application of variable-gain control techniques for high-performance motion systems". He is an IEEE Fellow for his contributions to hybrid, data-based and networked control.